CARBON XXX (2014) XXX–XXX

Available at www.sciencedirect.com

ScienceDirect

journal homepage: www.elsevier.com/locate/carbon

Enhanced lithiation in defective graphene

Dibakar Datta [a], *Junwen Li* [b], *Nikhil Koratker* [c,d,*], *Vivek B. Shenoy* [b,e,*]

[a] *School of Engineering, Brown University, Providence, RI 02912, United States*
[b] *Department of Materials Science and Engineering, University of Pennsylvania, Philadelphia, PA 19104, United States*
[c] *Department of Mechanical, Aerospace and Nuclear Engineering, Rensselaer Polytechnic Institute, Troy, NY 12180, United States*
[d] *Department of Materials Science and Engineering, Rensselaer Polytechnic Institute, Troy, NY 12180, United States*
[e] *Department of Mechanical Engineering and Applied Mechanics, University of Pennsylvania, Philadelphia, PA 19104, United States*

ARTICLE INFO

Article history:
Received 29 June 2014
Accepted 20 August 2014
Available online xxxx

ABSTRACT

We performed first-principle calculations based on density functional theory (DFT) to investigate adsorption of lithium (Li) on graphene with divacancy and Stone–Wales defects. Our results confirm that lithiation is not possible in pristine graphene. However, enhanced Li adsorption is observed on defective graphene because of the increased charge transfer between adatom and underlying defective sheet. Because of increased adsorption, the specific capacity is also increased with the increase in defect densities. For the maximum possible divacancy defect density, Li storage capacities of up to ~1675 mAh/g can be achieved. While for Stone–Wales defects, we find that a maximum capacity of up to ~1100 mAh/g is possible. Our results provide deeper understanding of Li-defect interactions and will help to create better high-capacity anode materials for Li-ion batteries.

1. Introduction

Rechargeable lithium ion batteries (LIBs) are driving a renaissance in electric-vehicle development, portable electronics, light vehicles, advanced energy storage systems and miscellaneous power devices [1]. The seemingly ubiquitous LIBs are the systems of choice, offering high energy density, flexible and lightweight design, and longer lifespan than comparable battery technologies [2,3]. However, as the global energy demand increases, developing new materials with higher charge capacity and better cycling performance for LIBs are of extreme importance [4]. Among the most intensively studied anode materials in LIBs are silicon and graphite [5]. Graphite is the widely used anode material in LIBs due to its high coulombic efficiency (the ratio of the number of charges that enter the battery during charging compared to the number that can be extracted from the battery during discharging) and excellent electrochemical stability [2]. However, its gravimetric capacity is relatively low (theoretical value of 372 mAh/g) leading to its limited performance in LIBs [2,6]. Compared to graphite, silicon offers ~10 times higher gravimetric energy densities as LIB anodes. However, this extremely high capacity of silicon is associated with massive structural changes and volume expansion on the order of 300%, resulting in electrode particle fracture, disconnection between the particles, capacity loss, and thus very limited cycle life [7]. Recent experimental studies show that low dimensional materials like graphene [8,9] and its oxide [10],

* *Corresponding authors:* Address: Department of Mechanical, Aerospace and Nuclear Engineering, Rensselaer Polytechnic Institute, Troy, NY 12180, United States (N. Koratker). Address: Department of Materials Science and Engineering, University of Pennsylvania, Philadelphia, PA 19104, United States (V.B. Shenoy).
E-mail addresses: koratn@rpi.edu (N. Koratker), vshenoy@seas.upenn.edu (V.B. Shenoy).
http://dx.doi.org/10.1016/j.carbon.2014.08.068
0008-6223/

carbon nanotubes [11,12], fullerenes [13], and silicon nanowires [14,15] offer higher specific capacities and could serve as a potential anode materials in LIBs.

Among the low dimensional materials, graphene, an atomic layer of carbon atoms arranged in a honeycomb lattice, is actively being pursued as a materials for next generation power devices since its discovery in 2004 [16]. Because of its superior electrical conductivity, high charge carrier mobility (20 $m^2 V^{-1} s^{-1}$), high surface area (2600 $m^2 g^{-1}$) and a broad electrochemical window [17,18], graphene can be particularly advantageous for its applications in energy storage devices [19], for example in LIBs [20,21]. However, impurities and defects (both vacancy and Stone–Wales) in graphene cannot be avoided [22,23] either because of the production process being used or because of the conditions under which the graphene device operates [24]. Recently, transmission electron microscopy (TEM) [25,26] and scanning tunneling microscopy (STM) [27,24] have been used to obtain images of defective graphene with atomic resolution [22]. Topological defects significantly influence the electronic, optical, mechanical, and thermal properties of graphene [22]. DFT studies [28] suggest that the intentional creation of point defects before absorbing Li would enhance adsorption significantly. In our recent paper [29], we have demonstrated this in terms of gravimetric capacity and investigated defect-induced plating of lithium metal within porous graphene networks. Despite studies on Li adsorption in defective graphene, several important questions remain unclear: What will be the lithiation and corresponding capacities for different percentages of divacancy (DV) and Stone–Wales (SW) defects? For different defect densities, what will be the maximum possible capacities? How exactly do lithium adatoms cluster on and around the defects? Which type of defect has the strongest influence on Li adsorption? Most importantly, what is the underlying mechanism of enhanced Li adsorption on graphene with structural defects? Recently, we have studied these issues for adsorption of Na and Ca to graphene surface [30]. In this study, we have performed first-principle calculations based on DFT to thoroughly investigate these questions for Li–graphene systems.

2. Computational models

All DFT calculations were performed using the Vienna Ab-initio Simulation Package (VASP) [31]. The detail methodology

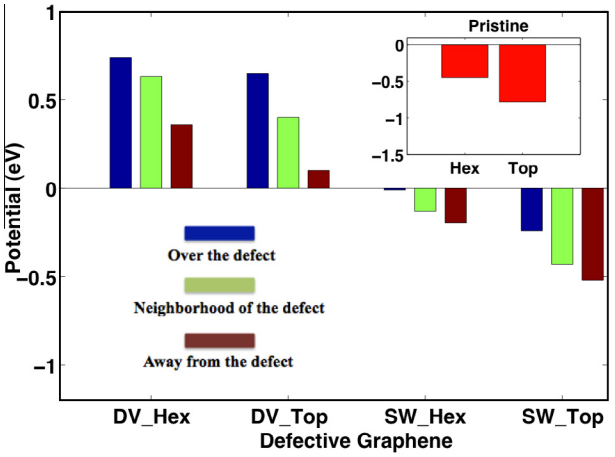

Fig. 2 – Lithiation potential for Li adsorption on different locations: pristine graphene (inset) and graphene with DV and SW defects at the Hex and Top sites. For each site, three positions, O (blue), N (green), and A (brown), are shown. (A color version of this figure can be viewed online.)

is explained in Supplementary Information. We consider here two kinds of structural defects: vacancy and Stone–Wales (SW). Among the vacancy defects, single vacancies (SV) with a carbon atom missing in graphene (or in the outermost layer of graphite) have been experimentally observed using TEM [25] and STM [27]. Because of geometry, one dangling bond always remains in the case of SV. On the other hand, for a divacancy (DV) defect, the edge is always saturated. As explained in our previous work [30], a DV is thermodynamically more favored over an SV and it is the most common type of vacancy defects observed experimentally [32,33]. A DV defect (shown in Fig. 1a) can be obtained by removing a C–C dimer from pristine graphene. Transmission electron microscopy (TEM) experiments frequently show the existence of both the 555-777 and 5-8-5 defects [34]. Stone–Wales defect is 55-77 defects and gives us an idea about the role of heptagon. So we selected 5-8-5 DV defect in order to include octagon in our studies. Moreover, octagonal defect has been extensively observed in experiments [35,32]. Electronics [36] and mechanical [37] properties of graphene with octagonal defect have been extensively studied and it has been found as source of gap states in graphene semiconducting

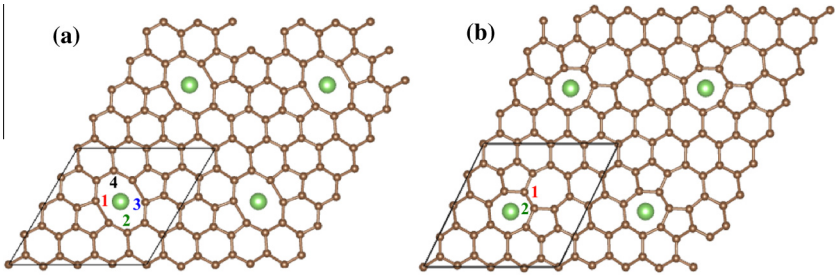

Fig. 1 – Graphene with (a) DV and (b) SW defect. Systems shown here are 2 × 2 super cell in size with periodicity in their in-plane dimensions. The super cell used in the calculation is marked in black. All systems are relaxed structure. Green indicates Li atom. (A color version of this figure can be viewed online.)

Please cite this article in press as: Datta D et al. Enhanced lithiation in defective graphene. Carbon (2014), http://dx.doi.org/10.1016/j.carbon.2014.08.068

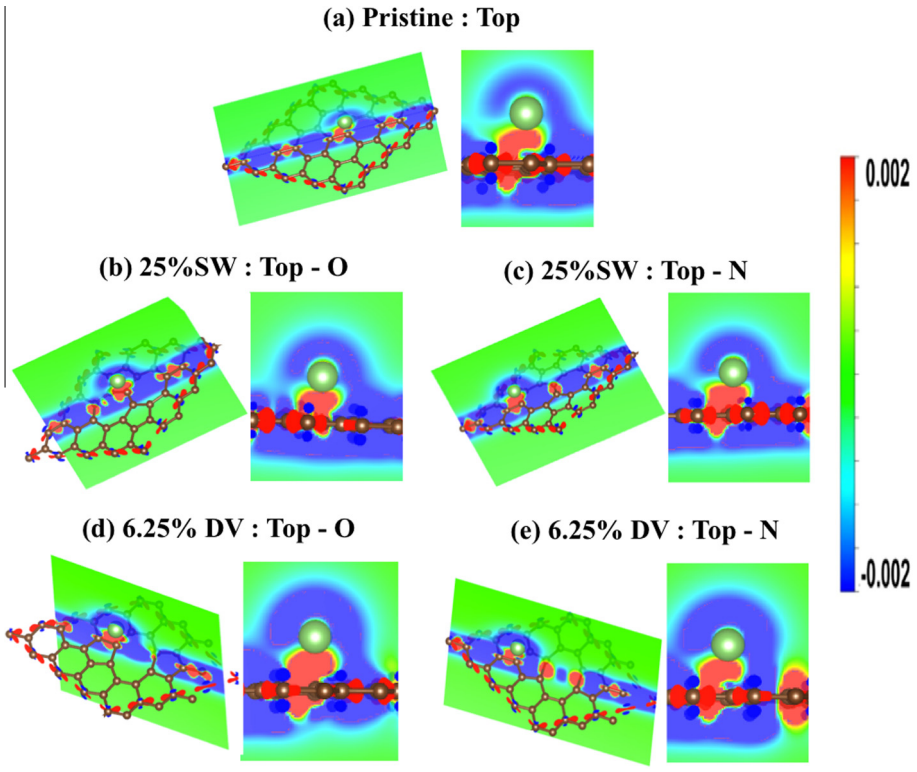

Fig. 3 – Bonding charge density for Li for (a) pristine, (b, c) Stone–Wales and (d, e) divacancy systems obtained as the charge-density difference between the valence charge density before and after bonding. Red and blue colors indicate the electron accumulation and depletion, respectively. The color scale is in the units of e/Bohr^3. (A color version of this figure can be viewed online.)

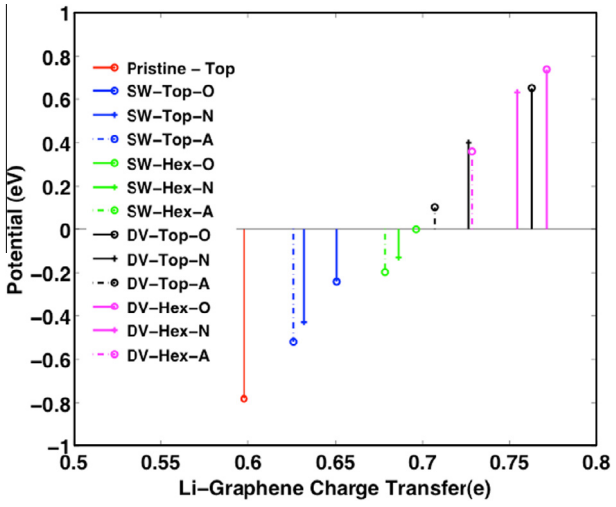

Fig. 4 – Charge-transfer vs lithiation potential. (A color version of this figure can be viewed online.)

structures [38]. For adsorption studies, octagonal defect has also been extensively considered [39,40]. Future research considering 555-777 DV defect will be interesting and should be pursued.

As shown in Supplementary Fig. S1, five different percentages of DV defects are considered: 6.25% (Fig. S1b), 12.50% (Fig. S1c), 16.00% (Fig. S1d), 18.75% (Fig. S1e), and 25.00% (Fig. S1f). Like DV, SW defect (Fig. 1b) is another common structural defect observed experimentally [41]. As shown in Supplementary Fig. S2, we have considered four types of SW defects with different concentration: 25% (Fig. S2a), 50% (Fig. S2b), 75% (Fig. S2c), and 100% (Fig. S2d). For 100% SW defect, we get the Haeckelite structure [42], which is a sheet full of 5–7 rings with the lowest equilibrium energy (the total ground-state energy) per carbon atom [30]. Apart from these defective structures, extensive research has been carried out on graphene with tilted Stone–Wales defect [43] and polycrystalline graphene [44]. These studies open many new windows: How will different orientations and tilting angle of SW defect affect Li adsorption? Can polycrystalline graphene be a potential anode material for LIBs? Future research to address these issues is warranted and should be pursued.

3. Results and discussion

3.1. *Analysis of adsorption potential for lowest defect density*

To get insight into adsorption of Li on defective structure, we first consider the lowest defect density *i.e.* 6.25% DV and 25% SW defect. The lattice constant of graphene is 2.46 Å [45,46]. Two sites of high symmetry for adsorption: the sites on the top of a carbon atom (Top) and the site at the center of a hexagon (Hex) of the graphene sheet are considered for detailed analysis of adsorption potential for these lowest

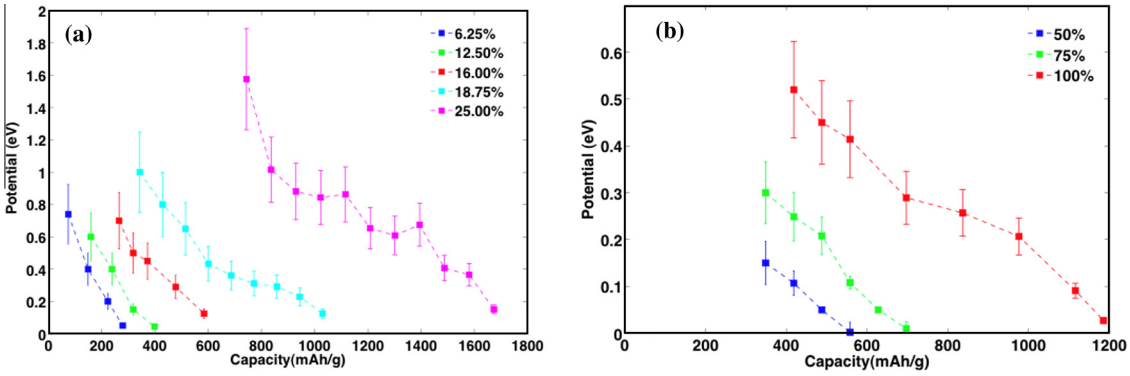

Fig. 5 – Capacity and corresponding lithiation potential for different percentages of (a) DV and (b) SW defects. (A color version of this figure can be viewed online.)

defect densities. For each site, we consider three positions: over the defect (O-position), neighborhood of the defect (N-position), and away from the defect (A-position). Supplementary Figs. S3 and S4 explain this concept of site and position that we have considered. As explained in detail in our previous work [30], regarding different available positions for adsorption, we select the location that has the maximum defective neighborhood (MDN). For example, as shown in Fig. 1a, considering the Top site at the O position (Top-O), we can place adatom on any of the eight carbons enclosing the octagon. However, a closer look at the geometry reveals that we have only two different options: location 1 and 2 or 3 and 4. Location 1 or 3 is at the junction of an octagon, hexagon and pentagon, whereas for location 2 or 4, it is at the junction of an octagon and two hexagons.

Fig. 2 shows the lithiation potential for three different positions (O, N, A) at both Hex and Top sites. Here negative potential indicates that adsorption is not possible. As indicated in inset in Fig. 2 (red), lithiation is not possible in case of pristine graphene [28]. However, presence of DV defects favor lithiation. O-position (blue) has maximum potential as it has MDN. Lithiation potential decreases form O to A positions. In case of SW defect, lowest defect density (25%) does not favor absorption for any positions. However, we notice that O-position is the most favorable position. This means, if we increase the defect density, it will favor adsorption. Hence we have considered higher defect densities *i.e.* 50%, 75%, and 100% for further calculation.

3.2. *Charge transfer analysis*

To get deeper physical insight into absorption, we performed bonding charge-density analysis [47]. Fig. 3 shows the bonding charge density passing through the bond between Li and the nearest carbon atom. The bonding charge density is obtained as the difference between the valence charge density of strain-free graphene–Li sheet and the superposition of valence charge density of the constituent atoms. A positive value (red) indicates electron accumulation, whereas a negative value (blue) denotes electron depletion. Changes in bonding charge distribution after introduction of defects clearly show that enhanced charge transfer from Li to underlying graphene sheet favors adsorption of adatom. To quantify the charge distribution, we performed Bader charge analysis [48]. Fig. 4 shows the charge transfer values for different defect sites and positions. The potential increases with increase in charge transfer. Beyond a threshold charge transfer of ~0.70*e*, Li adsorption is possible.

3.3. *Adsorption potential and capacities for different defect densities*

Analyzing Figs. 2–4, we notice that O position of Hex site (Hex-O) is the most favorable location of adsorption. Hence for initial distribution of Li, we have mainly focused on this location. For each defect density, to have certain capacity, we need adsorption of certain amount of Li adatoms. These adatoms can be placed over defective graphene in many different ways. For example, as shown Fig. S5, for 12.50% defect, we would like to have Li_5C_{28} (capacity = 398.4592 mAh/g) and Li_6C_{28} (capacity = 478.1510 mAh/g). As shown in upper and lower panel, lithium adatoms are placed in three different configurations. In fact, we can place adatoms in many other configurations *i.e. for every case; we have several options for the initial distribution*. For each configuration, adsorption potential

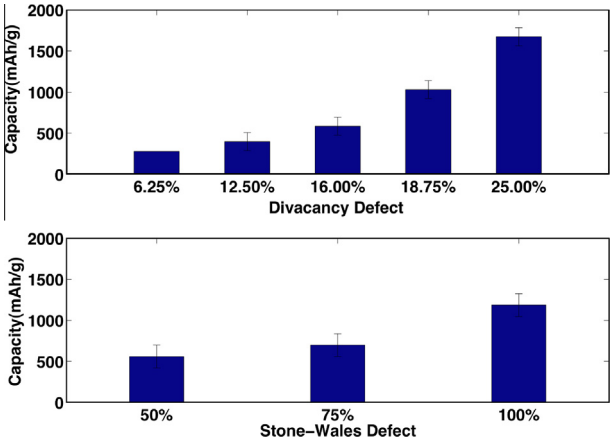

Fig. 6 – Maximum capacity for different DV and SW defect densities. (A color version of this figure can be viewed online.)

will be different. Naturally, if more adatoms are placed over and around the defect, potential will be more. If we compare configuration 1 and 2 in upper panel of Fig. S5, we notice for these cases, potentials are 0.0281 and 0.0523 eV respectively. For location 2, all adatoms are placed inside octagons while for location 1; one of them is placed outside resulting in lower potential. Likewise, as shown in Figs. S5–S11, for every case, we consider three among many possible configurations.

For each percentage of defects, we have carried out DFT calculations for different percentages of Li until adsorption is no longer possible *i.e.* potential becomes negative. Fig. 5a summarizes lithiation potential for five different DV defect densities. For highest defect density of 25% (Fig. S1f), we notice the formation of Li_3C_8 at a potential of 0.84 eV, corresponding to a maximum capacity of 837 mAh/g. The favorable formation of Li_3C_8 has been confirmed in our recent experimental studies [29]. Fig. 5b shows Li adsorption to defective graphene with SW defects. The results indicate significant Li absorption for 100% SW defects *i.e.* for the Haeckelite structure. Error bar of different height indicates the variation in potential range for different capacities. Fig. 6 summarizes the maximum capacity observed for different DV and SW defect densities. For highest DV defect of 25%, the maximum capacity is as high as ~1675 mAh/g, corresponding to a lithiation potential of ~0.1 eV. In the case of SW defects, we observe the highest capacity of ~1100 mAh/g for the Haeckelite structure.

4. Conclusions

In summary, we have performed first-principles calculations to investigate the Li adsorption on graphene with various DV and SW defect densities. We confirm that lithiation is not possible in pristine graphene. However, presence of defect favors adsorption. The potential is larger when adatom is on and around the defective zone. We have demonstrated the underlying charge-transfer mechanism for enhanced adsorption. Our results provide deeper insight into adsorption and will help to create better anode materials for higher capacity and better cycling performance for LIBs. In addition, since the charge transfer occurring in both defects is identified to account for the enhanced adsorption of Lithium, we hope this work will provide the first theoretical understanding on the experimentally observed lithiation and attract more researchers' attention on this important topic and promote the development of this field.

Acknowledgements

D.D., J.L., and V.B.S. gratefully acknowledge the support of the Army Research Office through contract W911NF-11-1-0171 and the National Science Foundation. N.K acknowledges funding support from the USA National Science Foundation (Award 0969895) and the John A. Clark and Edward T. Crossan Chair Professorship from the Rensselaer Polytechnic Institute. Authors would like to thank all three anonymous reviewers for their outstanding review that made our manuscript much better.

Appendix A. Supplementary data

Supplementary data associated with this article can be found, in the online version, at http://dx.doi.org/10.1016/j.carbon.2014.08.068.

REFERENCES

[1] Dahn JR, Zheng T, Liu YH, Xue JS. Mechanisms for lithium insertion in carbonaceous materials. Science 1995;270(5236):590–3.
[2] Tarascon JM, Armand M. Issues and challenges facing rechargeable lithium batteries. Nature 2001;414:359–67.
[3] Kim SP, Datta D, Shenoy VB. Atomistic mechanisms of phase boundary evolution during initial lithiation of crystalline silicon. J Phys Chem C 2014;118(31):17247–53.
[4] Miller JR, Simon P. Electrochemical capacitors for energy management. Science 2008;321(5889):651–2.
[5] Stournara ME, Guduru PR, Shenoy VB. Elastic behavior of crystalline Li–Sn phases with increasing Li concentration. J Power Sources 2012;208:165–9.
[6] Migge S, Sandmann G, Rahner D, Dietz H, Plieth W. Studying lithium intercalation into graphite particles via in situ Raman spectroscopy and confocal microscopy. J Solid State Electrochem 2005;9(3):132–7.
[7] Shenoy VB, Johari P, Qi Y. Elastic softening of amorphous and crystalline Li–Si phases with increasing Li concentration: a first-principles study. J Power Sources 2010;195(19):6825–30.
[8] Medeiros PVC, Mota FD, Mascarenhas AJS, de Castilho CMC. Adsorption of monovalent metal atoms on graphene: a theoretical approach. Nanotechnology 2010;21(11):115701.
[9] Romero MA, Garcia AI, Goldberg EC. Localized description of band structure effects on Li atom interaction with graphene. Phys Rev B 2011;83:125411.
[10] Stournara ME, Shenoy VB. Enhanced Li capacity at high lithiation potentials in graphene oxide. J Power Sources 2011;196(13):5697–703.
[11] Shimoda H, Gao B, Tang XP, Kleinhammes A, Fleming L, Wu Y, et al. Lithium intercalation into opened single-wall carbon nanotubes: storage capacity and electronic properties. Phys Rev Lett 2002;88(1):015502.
[12] Meunier V, Kephart J, Roland C, Bernholc J. *Ab initio* investigations of lithium diffusion in carbon nanotube systems. Phys Rev Lett 2002;88(7):075506.
[13] Buiel E, Dahn JR. Li-insertion in hard carbon anode materials for Li-ion batteries. Electrochim Acta 1999;45(1):121–30.
[14] Chan CK, Peng HL, Liu G, McIlwrath K, Zhang XF, Huggins RA, et al. High-performance lithium battery anodes using silicon nanowires. Nat Nanotechnol 2008;3(1):31–5.
[15] Chockla AM, Harris JT, Akhavan VA, Bogart TD, Holmberg VC, Steinhagen C, et al. Silicon nanowire fabric as a lithium ion battery electrode material. J Am Chem Soc 2011;133(51):20914–21.
[16] Novoselov KS, Geim AK, Morozov SV, Jiang D, Zhang Y, Dubonos SV, et al. Electric field effect in atomically thin carbon films. Science 2004;306(5696):666–9.
[17] Novoselov KS, Geim AK, Morozov SV, Jiang D, Katsnelson MI, Grigorieva IV, et al. Two-dimensional gas of massless Dirac fermions in graphene. Nature 2005;438(7065):197–200.
[18] Novoselov KS, Jiang Z, Zhang Y, Morozov SV, Stormer HL, Zeitler U, et al. Room-temperature quantum Hall effect in graphene. Science 2007;315(5817):1379.
[19] Wei D, Grande L, Chundi V, White R, Bower C, Andrew P, et al. Graphene from electrochemical exfoliation and its direct applications in enhanced energy storage devices. Chem Commun 2012;48(9):1239–41.

[20] Yoo E, Kim J, Hosono E, Zhou H, Kudo T, Honma I. Large reversible Li storage of graphene nanosheet families for use in rechargeable lithium ion batteries. Nano Lett 2008;8(8):2277–82.
[21] Jang BZ, Liu CG, Neff D, Yu ZN, Wang MC, Xiong W, et al. Graphene surface-enabled lithium ion-exchanging cells: next-generation high-power energy storage devices. Nano Lett 2011;11(9):3785–91.
[22] Banhart F, Kotakoski J, Krasheninnikov AV. Structural defects in graphene. ACS Nano 2011;5(1):26–41.
[23] Hashimoto A, Suenaga K, Gloter A, Urita K, Iijima S. Direct evidence for atomic defects in graphene layers. Nature 2004;430(7002):870–3.
[24] Zandiatashbar A, Lee GH, An SJ, Lee S, Mathew N, Terrones M, et al. Effect of defects on the intrinsic strength and stiffness of graphene. Nat Commun 2014;5(3186):1–9.
[25] Meyer JC, Kisielowski C, Erni R, Rossell MD, Crommie MF, Zettl A. Direct imaging of lattice atoms and topological defects in graphene membranes. Nano Lett 2008;8(11):3582–6.
[26] Kotakoski J, Krasheninnikov AV, Kaiser U, Meyer JC. From point defects in graphene to two-dimensional amorphous carbon. Phys Rev Lett 2011;106(10):105505.
[27] Ugeda MM, Brihuega I, Guinea F, Gomez-Rodriguez JM. Missing atom as a source of carbon magnetism. Phys Rev Lett 2010;104(9):096804.
[28] Zhou LJ, Hou ZF, Wu LM. First-principles study of lithium adsorption and diffusion on graphene with point defects. J Phys Chem C 2012;116(41):21780–7.
[29] Mukherjee R, Thomas AV, Datta D, Singh E, Li J, Eksik O, et al. Defect-induced plating of lithium metal within porous graphene networks. Nat Commun 2014;5(3710):1–10.
[30] Datta D, Li J, Shenoy VB. Defective graphene as a high-capacity anode material for Na- and Ca-ion batteries. ACS Appl Mater Interfaces 2014;6(3):1788–95.
[31] Kresse G, Furthmuller J. Efficient iterative schemes for ab initio total-energy calculations using a plane-wave basis set. Phys Rev B 1996;54(16):11169–86.
[32] Lahiri J, Lin Y, Bozkurt P, Oleynik II, Batzill M. An extended defect in graphene as a metallic wire. Nat Nanotechnol 2010;5(5):326–9.
[33] Carlsson JM, Scheffler M. Structural, electronic, and chemical properties of nanoporous carbon. Phys Rev Lett 2006;96(4):046806.
[34] Kim Y, Ihm J, Yoon E, Lee GD. Dynamics and stability of divacancy defects in graphene. Phys Rev B 2011;84(7).
[35] Yang B, Boscoboinik JA, Yu X, Shaikhutdinov S, Freund HJ. Patterned defect structures predicted for graphene are observed on single-layer silica films. Nano Lett 2013;13(9):4422–7.
[36] Okada S, Kawai T, Nakada K. Electronic structure of graphene with a topological line defect. J Phys Soc Jpn 2011;80(1):013709.
[37] Carpio A, Bonilla L. Periodized discrete elasticity models for defects in graphene. Phys Rev B 2008;78(8).
[38] Pelc M, Jaskólski W, Ayuela A, Chico L. Octagonal defects as the source of gap states in graphene semiconducting structures. Acta Phys Pol, A 2013;124(5):777–80.
[39] Oubal M, Picaud S, Rayez MT, Rayez JC. Adsorption of atmospheric oxidants at divacancy sites of graphene: a DFT study. Comput Theor Chem 2013;1016:22–7.
[40] Mehmood F, Pachter R, Lu W, Boeckl JJ. Adsorption and diffusion of oxygen on single-layer graphene with topological defects. J Phys Chem C 2013;117(20):10366–74.
[41] Reich S, Li L, Robertson J. Structure and formation energy of carbon nanotube caps. Phys Rev B 2005;72(16):165423.
[42] Terrones H, Terrones M, Hernandez E, Grobert N, Charlier JC, Ajayan PM. New metallic allotropes of planar and tubular carbon. Phys Rev Lett 2000;84(8):1716–9.
[43] He L, Guo S, Lei J, Sha Z, Liu Z. The effect of Stone–Thrower–Wales defects on mechanical properties of graphene sheets – a molecular dynamics study. Carbon 2014;75:124–32.
[44] Sha ZD, Pei QX, Liu ZS, Shenoy VB, Zhang YW. Is the failure of large-area polycrystalline graphene notch sensitive or insensitive? Carbon 2014;72:200–6.
[45] Fan X, Zheng WT, Kuo JL. Adsorption and diffusion of Li on pristine and defective graphene. ACS Appl Mater Interfaces 2012;4(5):2432–8.
[46] Yang CK. A metallic graphene layer adsorbed with lithium. Appl Phys Lett 2009;94(16):163115.
[47] Li J, Medhekar N, Shenoy VB. Bonding charge density and ultimate strength of monolayer transition metal dichalcogenides. J Phys Chem C 2013;117(30):15842–8.
[48] Tang W, Sanville E, Henkelman G. A grid-based Bader analysis algorithm without lattice bias. J Phys: Condens Matter 2009;21(8):084204.

Please cite this article in press as: Datta D et al. Enhanced lithiation in defective graphene. Carbon (2014), http://dx.doi.org/10.1016/j.carbon.2014.08.068

SUPPLEMENTARY INFORMATION

Methodology

All calculations are performed using the Vienna Ab Initio Simulation Package (VASP) [1] with the Projector Augmented Wave (PAW) [2,3] method and the Perdew-Burke-Ernzerhof (PBE) [4] form of the generalized gradient approximation (GGA) for exchange and correlation. For convergence studies, we determined a kinetic energy cut-off of 600 eV and a Fermi smearing width of 0.05 eV. The Brillouin zones of 4×4 and 5×5 super cell are sampled with the Γ-centered k-point grid of 9×9×1 and 7×7×1 respectively. In order to avoid the spurious coupling effect between graphene layers along the *z*-axis, the vacuum separation in the model structure is set to 18 Å. All atoms and cell-vectors are relaxed with a force tolerance of 0.02eV/Å.

The lithiation potential V is defined as [5,6]

$$V = -\frac{\Delta G_f}{z \bullet F} \qquad (1)$$

where F is the Faraday constant and z is the charge (in electrons) transported by lithium in the electrolyte. In most nonelectronically conducting electrolytes $z = 1$ for Li intercalation. The change in Gibb's free energy is

$$\Delta G_f = \Delta E_f + P\Delta V_f - T\Delta S_f \qquad (2)$$

Since the term $P\Delta V_f$ is of the order of 10^{-5} eV[5], whereas the term $T\Delta S_f$ is of the order of the thermal energy (26 meV at room temperature), the entropy and the pressure terms can be neglected and the free energy will be approximately equal to the formation energy ΔE_f obtained from DFT calculations. The formation energy is defined as

$$\Delta E_f = E_{Li_nG} - (nE_{Li} + E_G) \qquad (3)$$

where n is the number of Li atoms inserted in the computational cell, E_{Li_nG} is the total energy of the Lithiated Graphene (Li_nG) structure, E_{Li} is the total energy of a single Li atom in elemental body-centered cubic Li, and E_G is the total energy of a particular graphene structure. From DFT calculation, we have obtained E_{Li} to be -1.8978 eV. If the energies are expressed in electron volts, the potential of the Li_nG structures vs. $Li/Li+$ as a function of lithium content can be shown as [7]

$$V = -\frac{\Delta E_f}{n} \qquad (4)$$

The composition range over which Li can be reversibly intercalated determines the battery capacity.

In our calculations, we have included spin polarization but not the van der Waals (VdW) interaction. The inclusion of VdW interaction is expected to affect our results based on PBE. But the charge transfer mechanism underlying the enhanced adsorption will remain unchanged. Since VdW interaction gives rise to stronger binding, its inclusion will lead to higher capacities. However, overall trend or major conclusion of this work will remain the same.

References

[1] Kresse G, Furthmuller J. Efficient iterative schemes for ab initio total-energy calculations using a plane-wave basis set. Phys Rev B 1996;54(16):11169-86.

[2] Kresse G, Joubert D. From ultrasoft pseudopotentials to the projector augmented-wave method. Phys Rev B 1999;59(3):1758-75.

[3] Blochl PE. Projector augmented-wave method. Phys Rev B Condens Matter 1994;50(24):17953-79.

[4] Perdew JP, Burke K, Wang Y. Generalized gradient approximation for the exchange-correlation hole of a many-electron system. Phys Rev B 1996;54(23):16533-39.

[5] Aydinol MK, Ceder G. First-principles prediction of insertion potentials in Li-Mn oxides for secondary Li batteries. J Electrochem Soc 1997;144(11):3832-35.

[6] Stournara ME, Shenoy VB. Enhanced Li capacity at high lithiation potentials in graphene oxide. Journal of Power Sources 2011;196(13):5697-5703.

[7] Aydinol MK, Kohan AF, Ceder G, Cho K, Joannopoulos J. Ab initio study of lithium intercalation in metal oxides and metal dichalcogenides. Phys Rev B 1997;56 (3):1354-65.

FIGURES

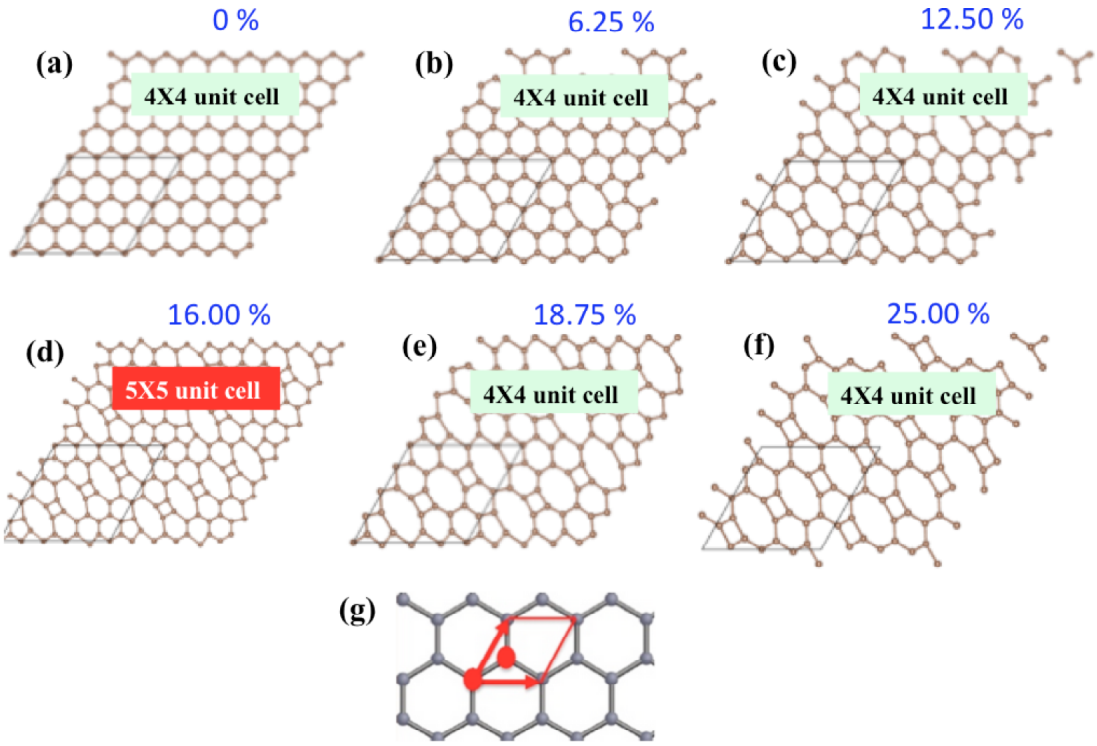

Figure S1: (a) Pristine graphene and graphene with DV defects (b) 6.25, (c) 12.50, (d) 16.00, (e) 18.75, (f) 25.00%. Systems shown here are 2X2 super cell in size with periodicity in their in-plane dimensions. For 16% defect, super cell is composed of 5X5 unit cell. For remaining cases, 4X4 unit cell is used. The super cell used in the calculation is marked in black. All systems are relaxed structure. (g) Unit cell considered creating the structure. One unit cell consists of 2 atoms.

In this study, we have considered triclinic system instead of square sheet. Since we are considering periodic systems *i.e.* there is no edge stress, overall conclusions for triclinic and square sheet will be same. To generate triclinic super cell, we used unit cell consisting of 2 atoms. For square sheet, we need unit cell consisting at least 4 atoms. For

DFT computation, we are using VASP package, which cannot handle too many atoms. For computational efficiency, it is desirable to have less number of atoms. Therefore, it is better to consider unit cell with less number of atoms.

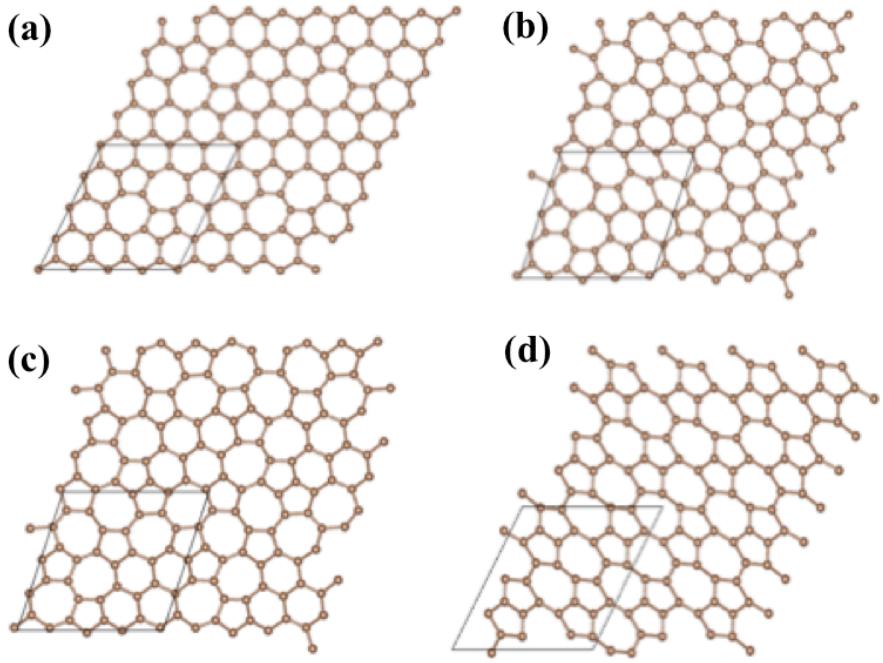

Figure S2: Graphene with SW defects (a) 25, (b) 50, (c) 75, (d) 100%. Systems shown here are 2X2 super cell in size with periodicity in their in-plane dimensions. The super cell used in the calculation is marked in black. All systems are relaxed structure.

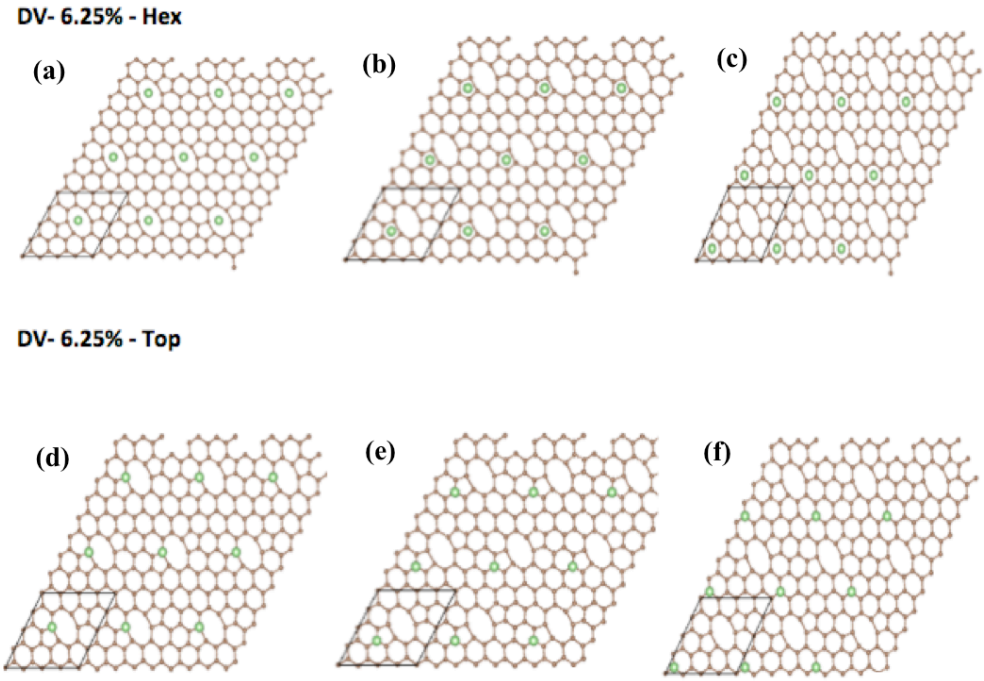

Figure S3: Li adsorption on DV Hex (a-c) and Top (d-f) site at (a,d) over the defect (O position) (b,e) neighborhood of the defect (N position) and (c,f) away from the defect (N position).

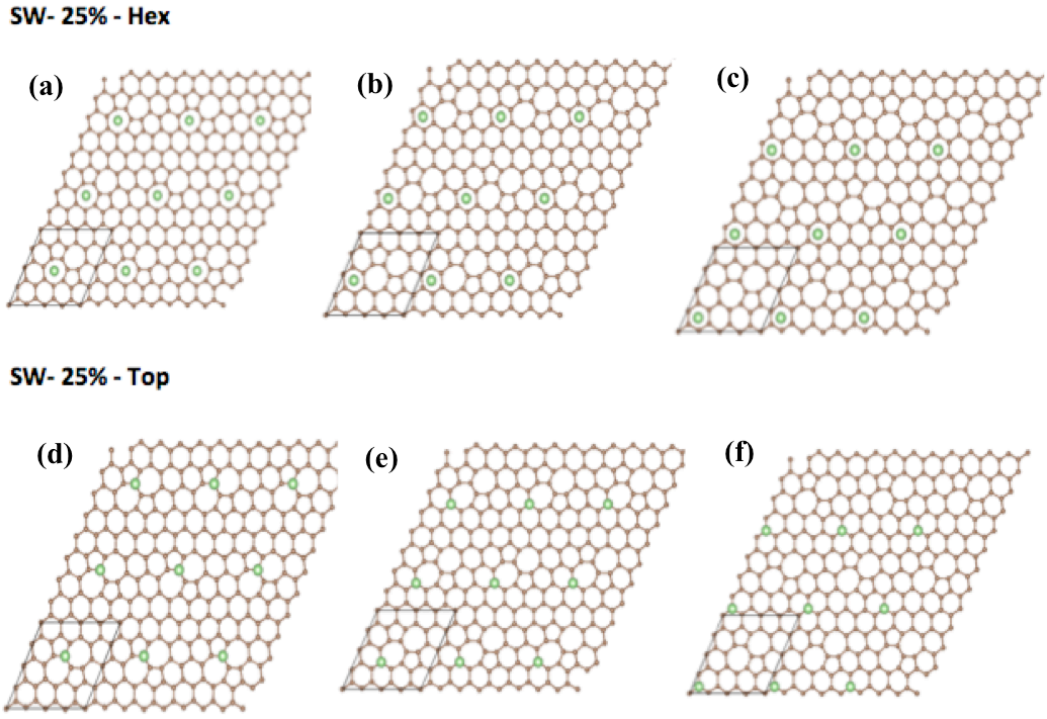

Figure S4: Li adsorption on SW Hex (a-c) and Top (d-f) site at (a,d) over the defect (O position) (b,e) neighborhood of the defect (N position) and (c,f) away from the defect (N position).

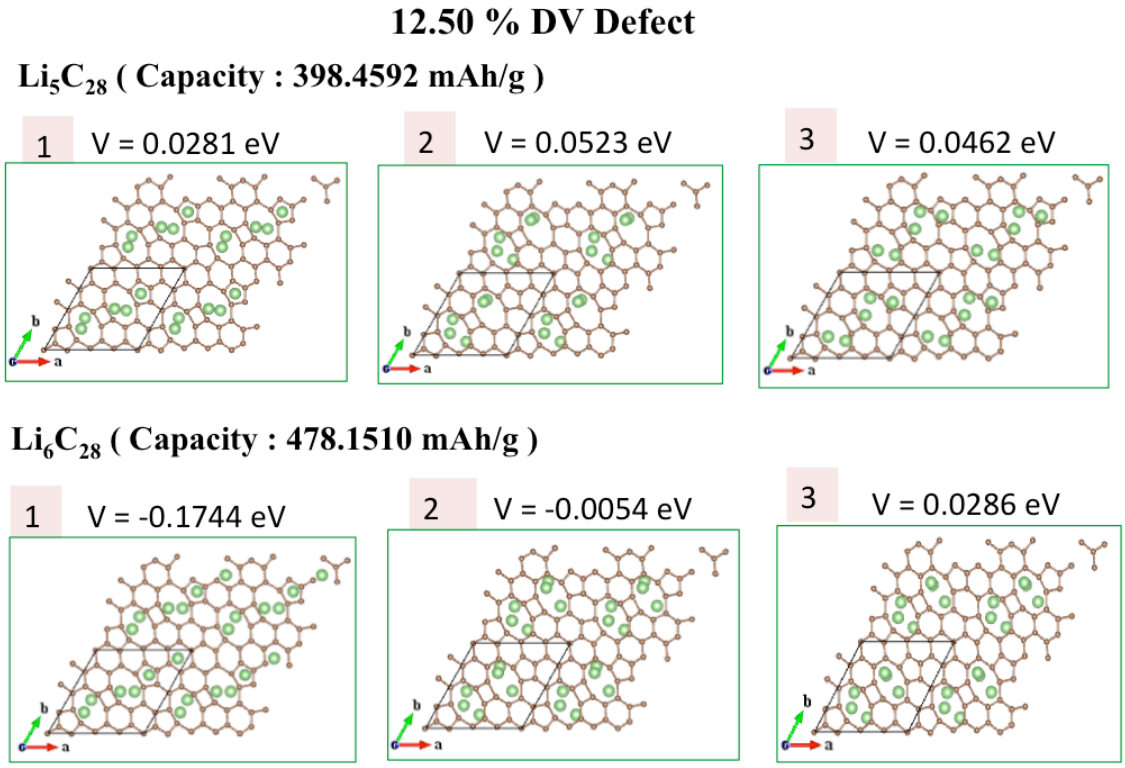

Figure S5: Different relaxed configurations of Li_5C_{28} and Li_6C_{28} for 12.50% divacancy defect.

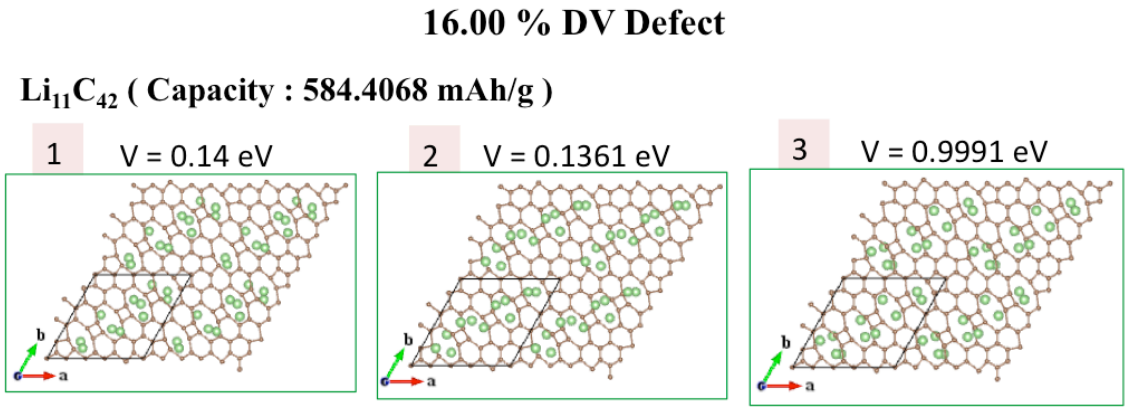

Figure S6: Different relaxed configurations of $Li_{11}C_{42}$ for 16.00% divacancy defect.

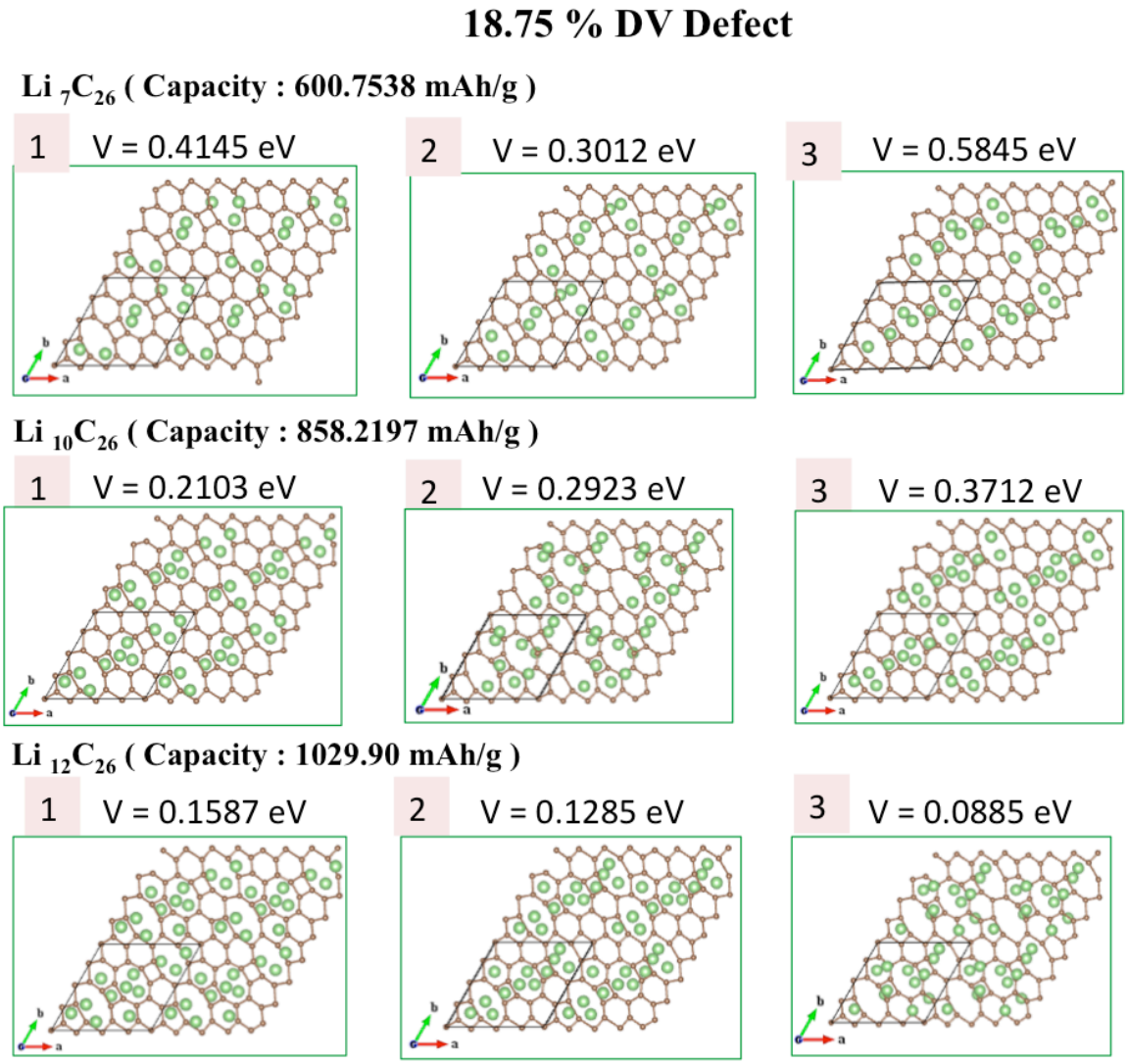

Figure S7: Different relaxed configurations of Li_7C_{26}, $Li_{10}C_{26}$, and $Li_{12}C_{26}$ for 18.75% divacancy defect.

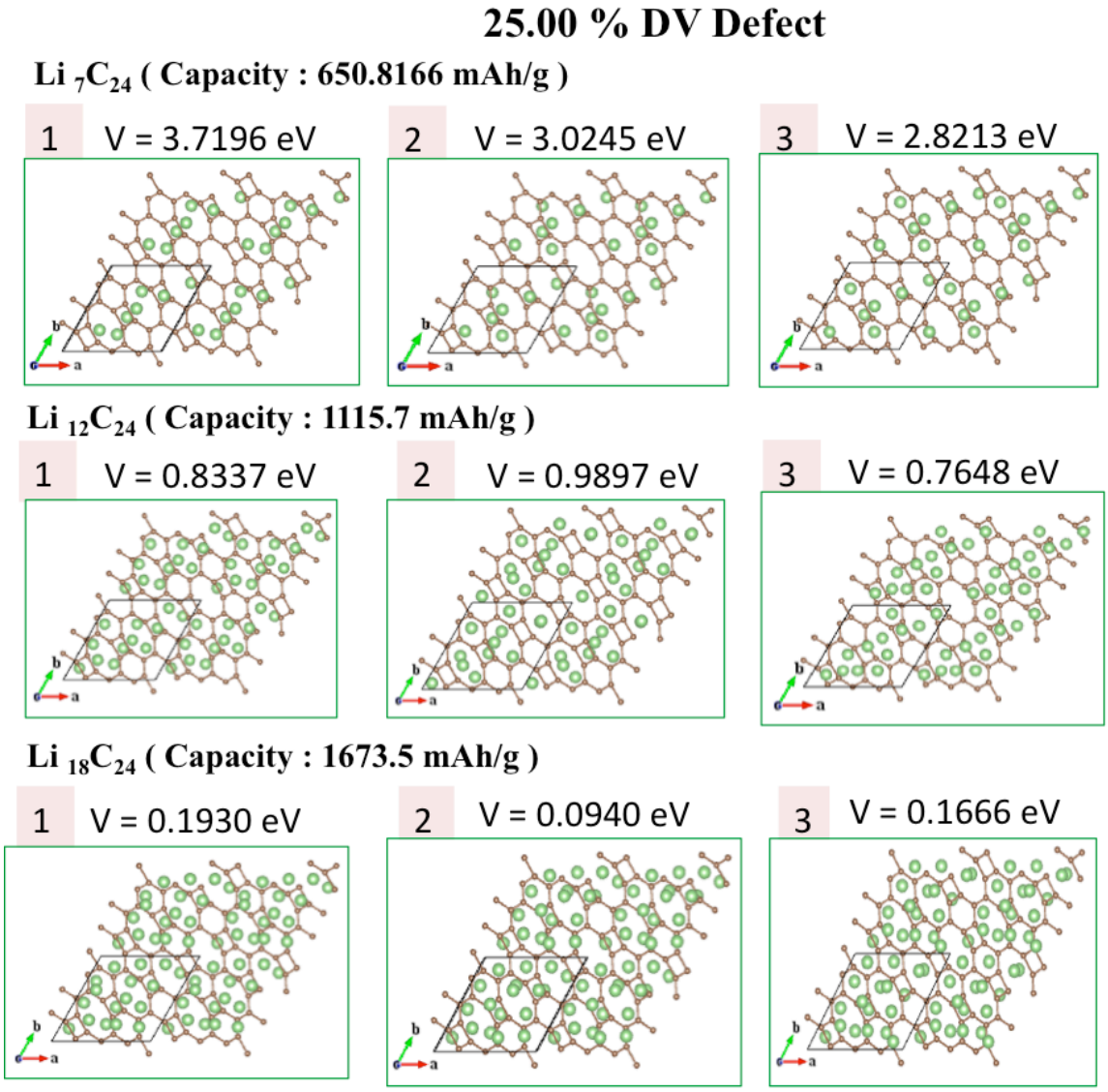

Figure S8: Different relaxed configurations of Li_7C_{24}, $Li_{12}C_{24}$, and $Li_{18}C_{24}$ for 25.00% divacancy defect.

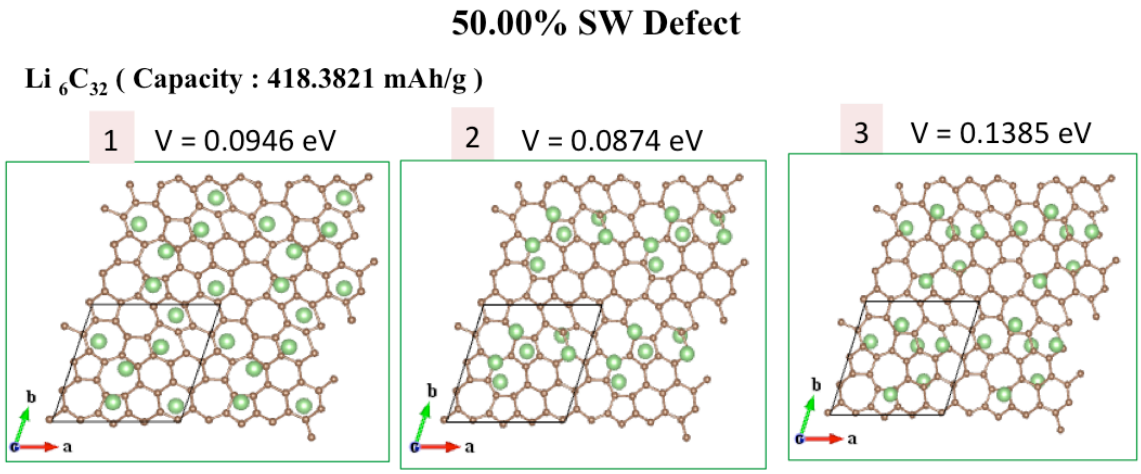

Figure S9: Different relaxed configurations of Li_6C_{32} for 50.00% SW defect.

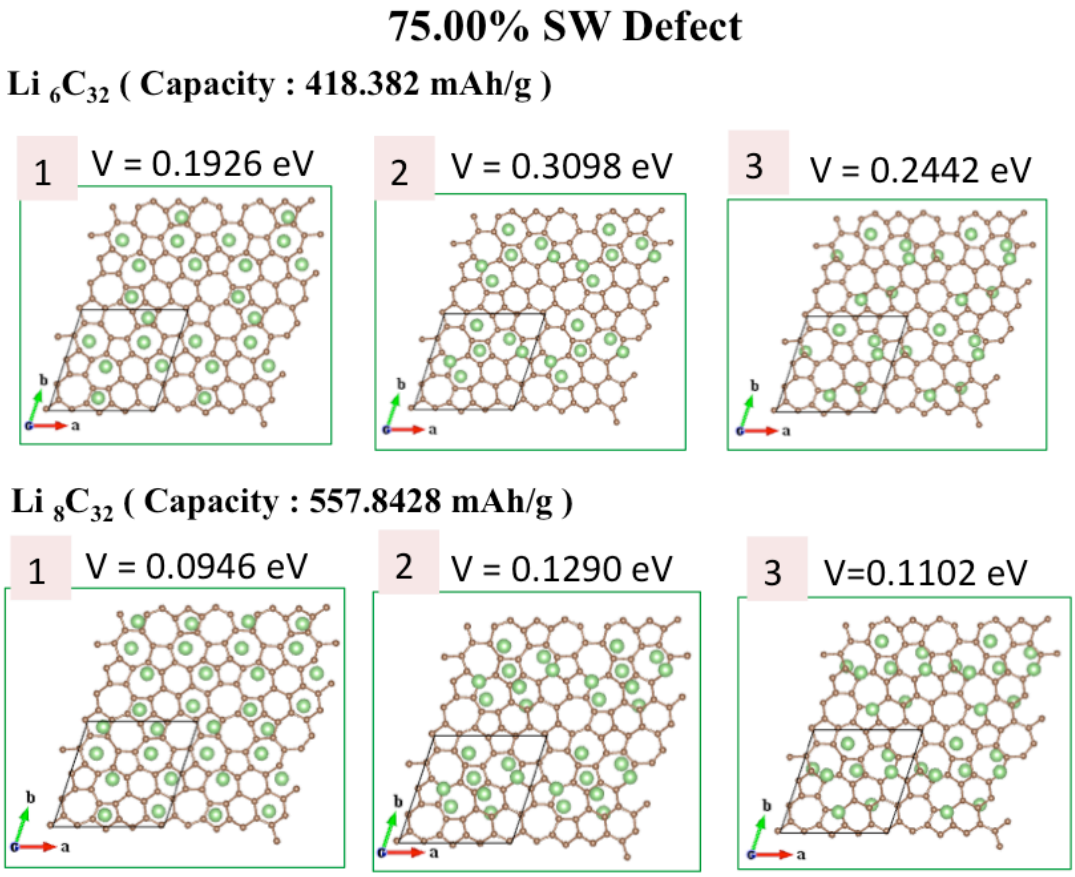

Figure S10: Different relaxed configurations of Li_6C_{32} and Li_8C_{32} for 75.00% SW defect.

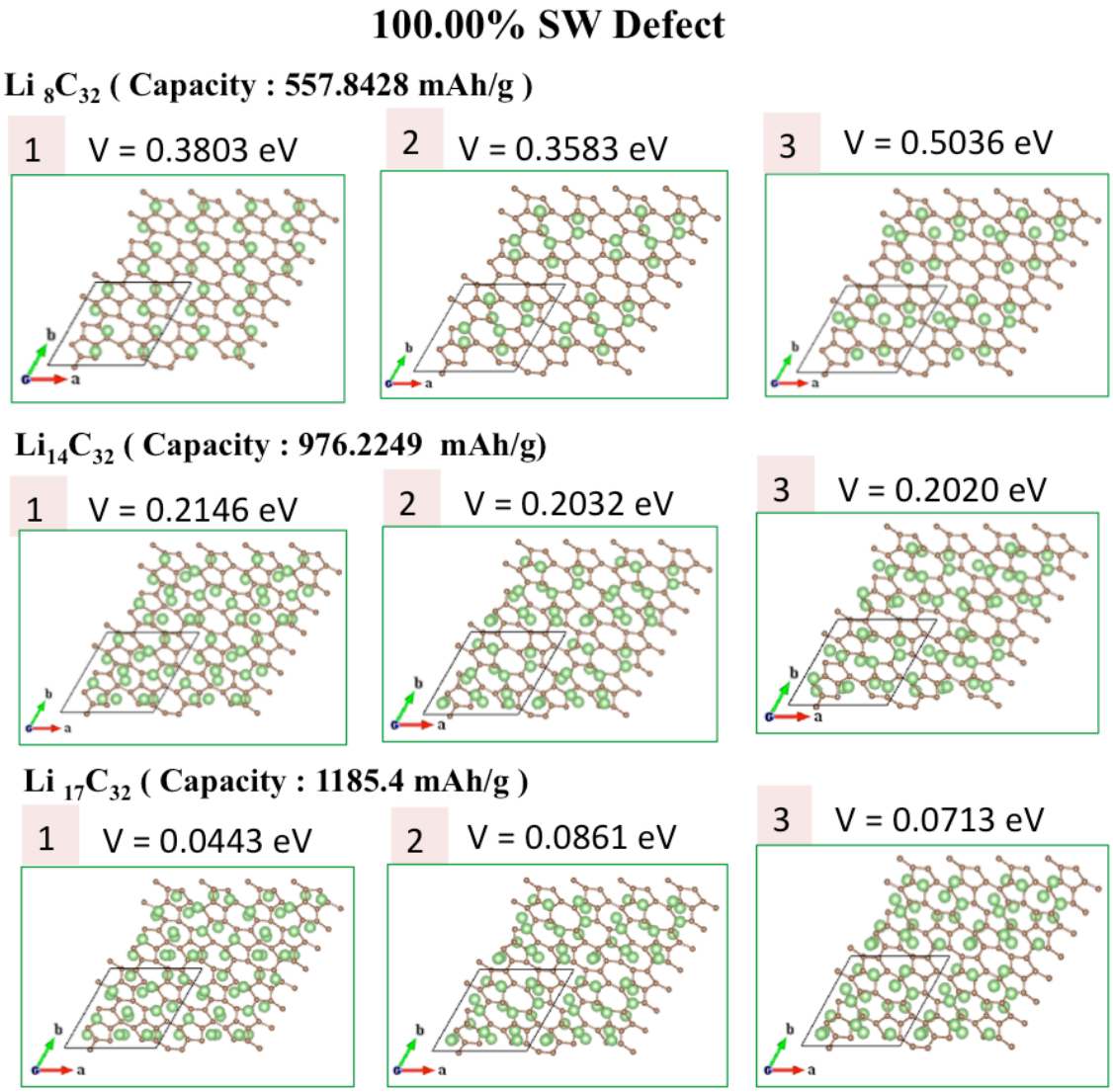

Figure S11: Different relaxed configurations of Li_8C_{32}, $Li_{14}C_{32}$ and $Li_{17}C_{32}$ for 100.00% SW defect.

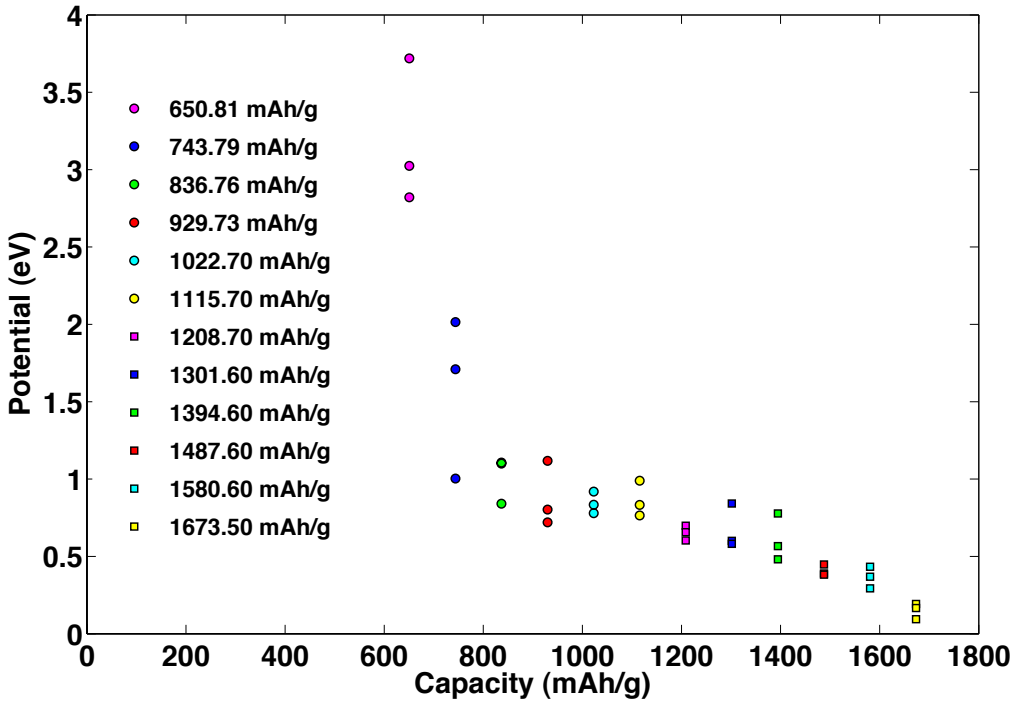

FIGURE S12: Lithiation potential for different capacity for 25% DV defect. Here three points at each capacity corresponds to three different initial configurations.